atmosphere

MDPI

*Article*

# Supplementary Materials: Modelling of Deep Street Canyon Air Pollution Chemistry and Transport: A Wintertime Naples Case Study

**Yuqing Dai [1], Andrea Mazzeo [1,2], Jian Zhong [1], Xiaoming Cai [1], Benedetto Mele [3], Domenico Toscano [4], Fabio Murena [4] and A. Rob MacKenzie [1,*]**

[1] School of Geography Earth and Environment Sciences, University of Birmingham, Birmingham B15 2TT, UK; yxd598@student.bham.ac.uk (Y.D.); j.zhong.1@bham.ac.uk (J.Z.); caixm99@gmail.com (X.C.)
[2] Lancaster Environment Centre, Lancaster University, Lancaster LA14YQ, UK; a.mazzeo@lancaster.ac.uk (A.M.)
[3] Department of Industrial Engineering, University of Naples Federico II, P.le V. Tecchio 80, 80125 Naples, Italy; benmele@unina.it;
[4] Department of Chemical, Materials and Production Engineering, University of Naples Federico II, P.le V. Tecchio 80, 80125 Naples, Italy. domenico.toscano@unina.it (D.T.); murena@unina.it (F.M.)
* Correspondence: a.r.mackenzie@bham.ac.uk

## Supplementary Materials: Comparing MBM-FleX and MBM-FleX_r results with CFD data

This study involved conducting model evaluations for MBM-FleX_r by comparing it to its origin version, MBM-FleX, and LES results. The model's initial and background conditions, emissions, and other configurations, along with operational procedures, have been kept consistent with our prior work (c.f., Dai, Cai, Zhong and MacKenzie [12]). Here, some briefings were summarized: the box-dimensions for MBM-FleX/MBM-FleX_r are 4 × 4 for the regular canyon (AR = 1) and 4 × 8 for the deep canyon (AR = 2), respectively; the prevailing wind speed is 2 m $s^{-1}$; exchange velocities $w_{e,0}$ are 0.021 m $s^{1}$ and 0.012 m $s^{-1}$ for regular and deep canyons, respectively [1,2]; a simple $NO_x$-$O_3$ chemistry with a *J*-value of $9.20 \times 10^{-3}$ $s^{-1}$ for $NO_2$ photodegradation, and a reduced chemical scheme (RCS) with 51 species and 136 reactions including hydroperoxyl radical chemistry are adopted [1]. The RCS explicitly incorporated inorganic chemistry from a more comprehensive chemical scheme Master Chemical Mechanism (MCM) and maintained OH levels within 10% of those predicted by the full MCM.

Figures S3 and S4 show the results of different air quality models for an idealized regular canyon (AR = 1) using the simple $NO_x$-$O_3$ chemistry and reduced chemical scheme (RCS) chemistry. Meanwhile, Figures S5 and S6 show the result of two chemical schemes for a deep canyon (AR = 2), respectively. In the regular canyon, the spatial distribution of a chemically inert passive tracer (PS) exhibited good agreements between MBM-FleX and LES models, and our prior work [3] provides detailed discussions of the results. The modified version of MBM-FleX (MBM-FleX_r) presented comparable performance to the original MBM FleX and LES on the leeward side. The model exhibited a tendency to overestimate passive tracer (PS) concentrations along the windward side of the canyon; for instance, the overestimation amounted to approximately 17% in the case of a standard canyon, and 12% for a deep canyon configuration. This discrepancy can be attributed to the significant influence of urban background factors on the location at the windward crest of buildings, that is, employing an averaging-flux approach for the entire street canyon may consequently result in an underestimation of the impact of fresh air influx into the canyon. For reactive species, MBM-FleX_r with the simple $NO_x$-$O_3$ chemistry

overestimated $NO_2$ concentrations, with the largest differences occurring on the windward side of the canyon (i.e., 14 ppb and 35 ppb for regular and deep canyons, respectively). $O_3$ was overestimated on the leeward side (~1 ppb) but was underestimated on the windward side (~3 ppb) due to the complex dynamics and segregation effects in chemistry [4,5]. VOC chemistry, to some extent, amplified these differences as shown in Figure S3. Moreover, MBM-FleX_r tended to underestimate PS concentrations at the pedestrian level in the deep canyon, with the degree of underestimation reducing with increasing building height. Eventually, MBM-FleX_r-modelled PS surpassed those of LES on the windward roof. $NO_2$ and $O_3$ showed a tendency to overestimate. The differences between MBM-FleX_r and MBM-FleX/LES become more significant on the leeward side for $O_3$ and on the windward side for $NO_2$, possibly due to uncertainties in representing tightly coupled physical and chemical processes. MBM-FleX_r can also reproduce the spatial distribution of air pollution within urban canyons and agreed well with LES, though it lost some accuracy compared to its original version MBM-FleX. Both the MBM-FleX and MBM-FleX_r for simulations in the real canyon following parameter evaluations were employed to further assess model applicability.

There are some challenges in dynamic parameter derivation processes. These parameters employed by the multi-box models are derived from CFD simulations. For every new modelling scenario, there is an imperative to initiate CFD in order to furnish the necessary data for multi-box model parameter estimations. Moreover, the measured data often displays pronounced variability, shaped by oscillating meteorological conditions, emission origins, and additional external variables. Assimilating this multifaceted data into an integrated model introduces its own array of complexities.

## Supporting Figures

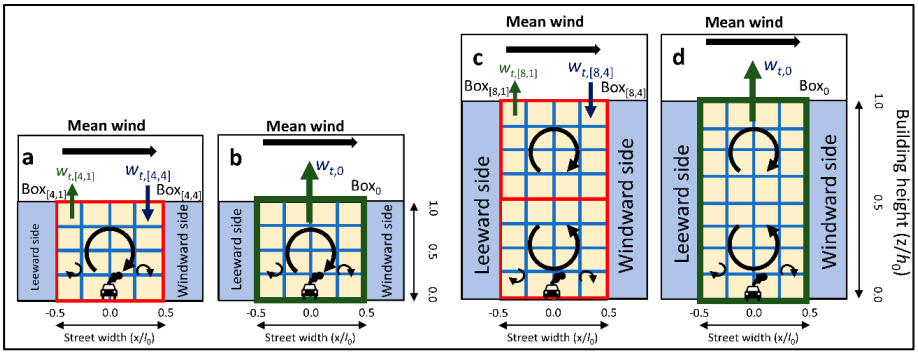


**Figure S1.** Diagram of the multi-box model (MBM-FleX) for air quality simulation within (**a**,**b**) regular and (**c**,**d**) deep street canyons. Red frames represent compartments that resolve a large vortex, blue lines further split the canyon volume into finer boxes, indicating the spatial resolution of the model within canyons, and green frame represents the entire volume of street canyons.

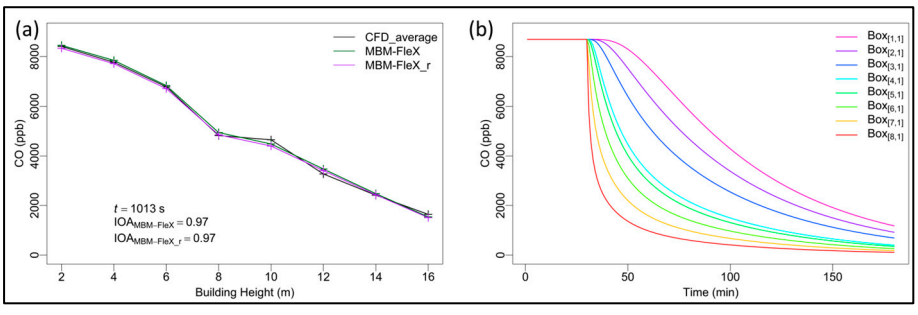


**Figure S2.** Model results of CO concentrations from MBM-FleX, MBM-FleX_r, and CFD (i.e., RANS) for a deep canyon (AR = 3), where (**a**) shows the vertical distributions of CO concentrations within the canyon, and (**b**) illustrates the dissipation rates of CO with time.

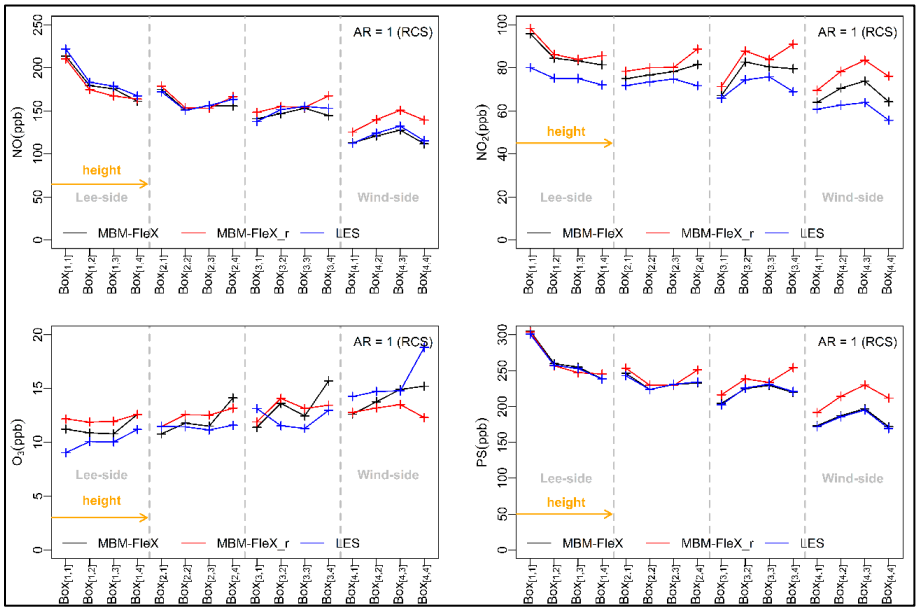


**Figure S3.** Model results of NO, $NO_2$, $O_3$, and PS from the original (i.e., MBM-FleX), revised (e.g., MBM-FleX_r) multi-box models, and large-eddy simulations (LES) with the simple $NO_x$-$O_3$ chemistry for the regular canyon (AR = 1). The black line represents results from MBM-FleX, the red line represents results from MBM-FleX_r, and the blue line represents results from LES, respectively. The grey dashed lines represent the division of the canyon horizontally, from the lee-side to the wind-side; in each panel the height increases as indicated by the orange arrow.

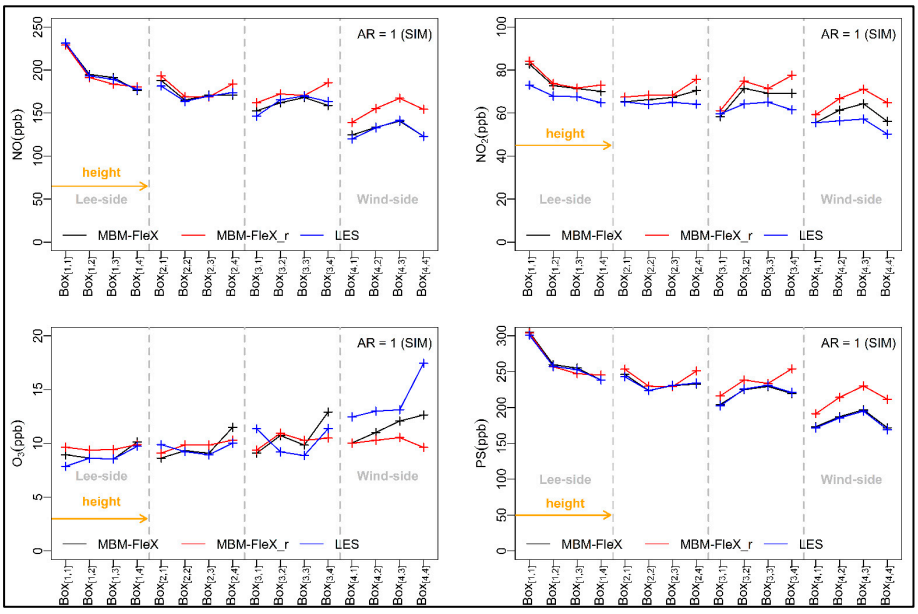


**Figure S4.** Model results of NO, $NO_2$, $O_3$, and PS from the original (i.e., MBM-FleX), revised (e.g., MBM-FleX_r) multi-box models, and large-eddy simulations (LES) with the reduced chemical scheme (RCS) for the regular canyon (AR = 1). The black line represents results from MBM-FleX, the red line represents results from MBM-FleX_r, and the blue line represents results from LES, respectively. The grey dashed lines represent the division of the canyon horizontally, from the lee-side to the wind-side; in each panel the height increases as indicated by the orange arrow.

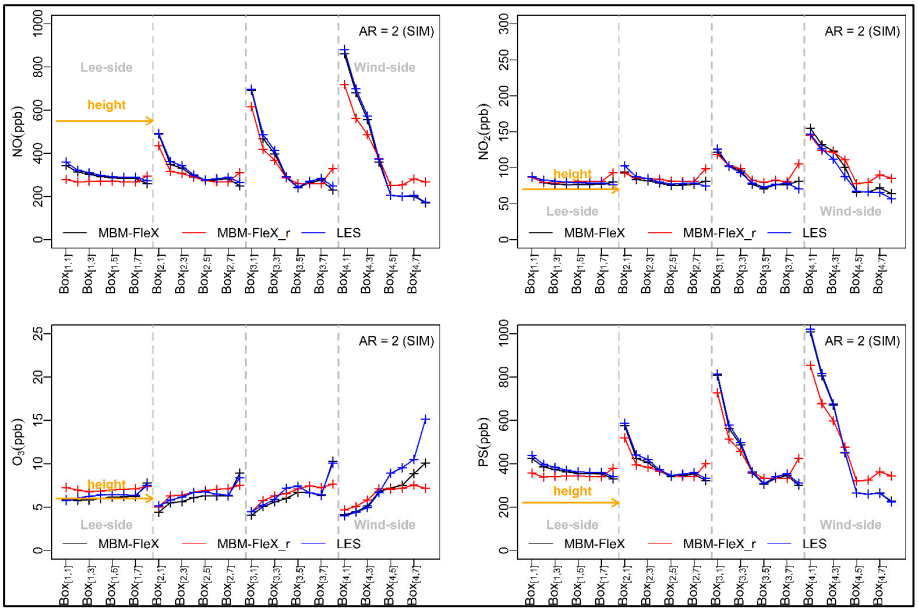


**Figure S5.** Model results of NO, $NO_2$, $O_3$, and PS from the original (i.e., MBM-FleX), revised (e.g., MBM-FleX_r) multi-box models, and large-eddy simulations (LES) with the simple $NO_x$-$O_3$ chemistry for the regular canyon (AR = 1). The black line represents results from MBM-FleX, the red line represents results from MBM-FleX_r, and the blue line represents results from LES, respectively. The grey dashed lines represent the division of the canyon horizontally, from the lee-side to the wind-side; in each panel the height increases as indicated by the orange arrow.

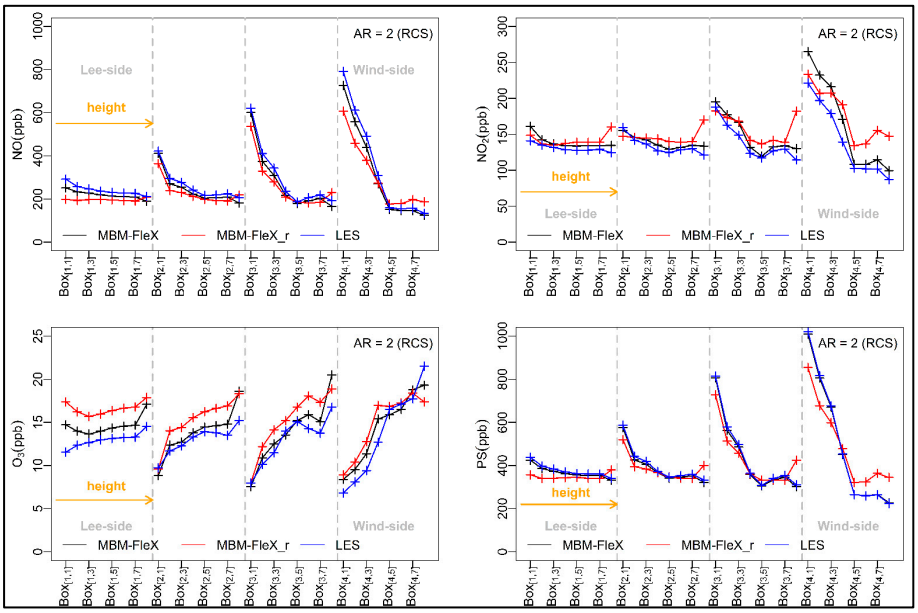


**Figure S6.** Model results of NO, $NO_2$, $O_3$, and PS from the original (i.e., MBM-FleX), revised (e.g., MBM-FleX_r) multi-box models, and large-eddy simulations (LES) with reduced chemical scheme (RCS) for the deep canyon (AR = 2). The black line represents results from MBM-FleX, the red line represents results from MBM-FleX_r, and the blue line represents results from LES, respectively. The grey dashed lines represent the division of the canyon horizontally, from the lee-side to the wind-side; in each panel the height increases as indicated by the orange arrow.

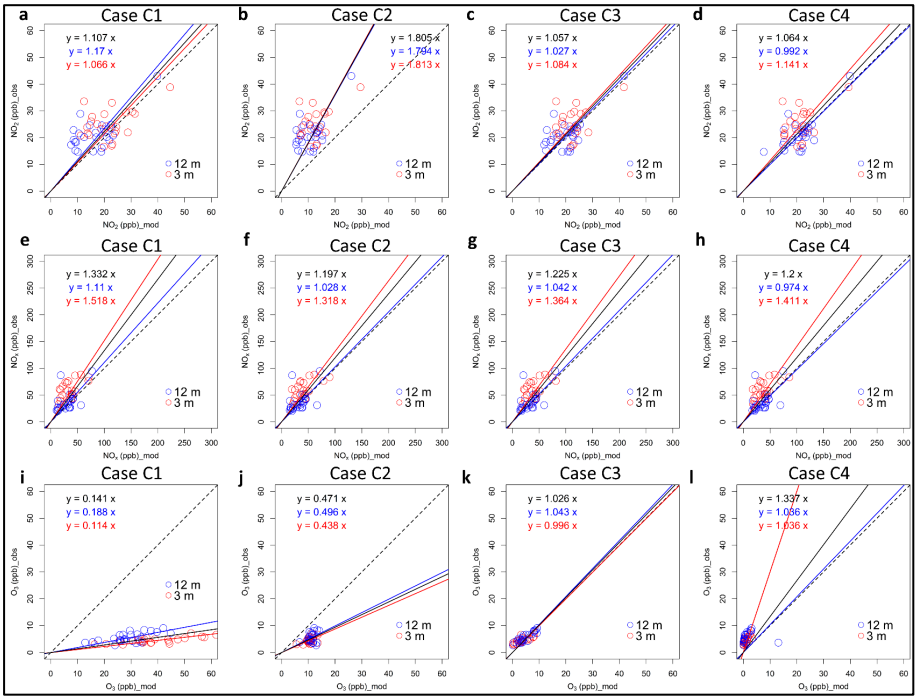


**Figure S7.** Scatter plot illustrating the correlation between modeled (MBM-FleX_r) and observed $NO_2$, $NO_x$, and $O_3$ concentrations at various heights within the deep street canyon. The red line delineates the relationship between modeled and observed values at 3 m height, the blue line represents the relationship at 12 m height, and the black line signifies model evaluations using data from all heights.

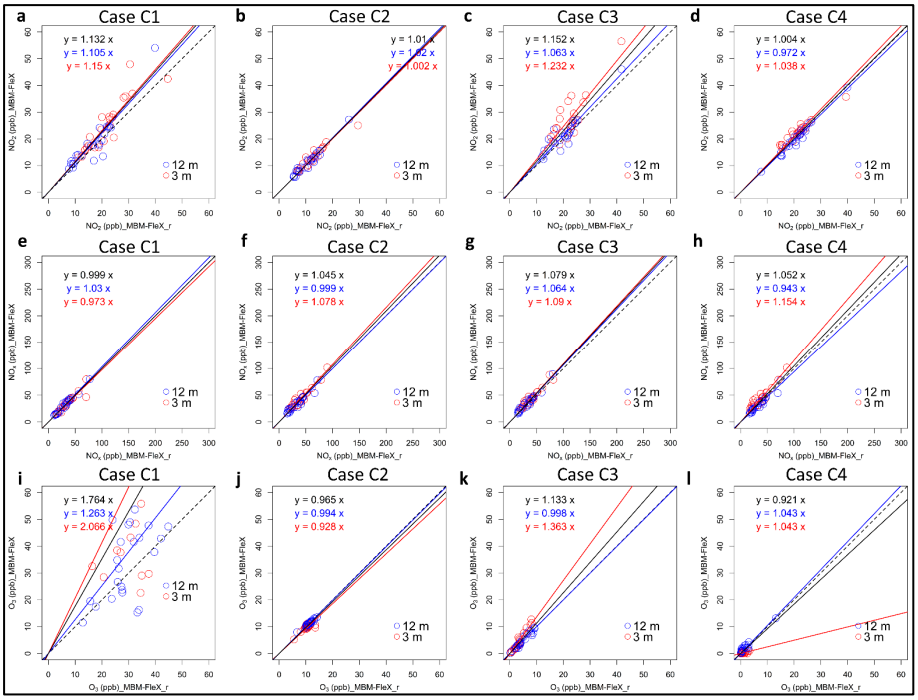


**Figure S8.** Scatter plot illustrating the correlation between MBM-FleX_r and MBM-FleX simulations at various heights within the deep street canyon. The red line delineates the relationship between modeled and observed values at 3 m height, the blue line represents the relationship at 12 m height, and the black line signifies model evaluations using data from all heights.

## Supporting Tables

**Table S1.** Turbulent mixing velocities used in the MBM-FleX/MBM-FleX_r model, these dynamical parameters are derived from wash-out CFD simulations for a deep canyon (AR = 3) under a prevailing wind speed of 2 m $s^{-1}$ in the neutral atmosphere.

| **Vertical Turbulence (m $s^{-1}$)** | |
|---|---|
| $w_t$ = 3.2e-04 | $w_t$ = 3.2e-04 |
| $w_{e\,[2,1]}$ = 3.92e-03 | $w_{e\,[2,1]}$ = 3.92e-03 |
| $w_{e\,[3,1]}$ = 2.4e-04 | $w_{e\,[3,1]}$ = 2.4e-04 |
| $w_{e\,[4,1]}$ = 1.99e-02 | $w_{e\,[4,1]}$ = 1.99e-02 |
| $w_{e\,[5,1]}$ = 2.76e-02 | $w_{e\,[5,1]}$ = 2.76e-02 |

**Table S2.** Emission factors of main vehicle categories were calculated using the COPERT procedure at 20 km $h^{-1}$, the unit has been transformed from g $km^{-1}$ $h^{-1}$ into ppb according to the volume of model mesh under standard pressure and 293 K.

| Category | CO | | $NO_x$ | | VOCs | | Primary $NO_2$ |
|---|---|---|---|---|---|---|---|
| | g $km^{-1}$ $h^{-1}$ | ppb $s^{-1}$ | g $km^{-1}$ $h^{-1}$ | $ppb^{-1}$ | g $km^{-1}$ $h^{-1}$ | $ppb^{-1}$ | $NO_2/NO_x$ |
| Buses | 2.93 | 0.104 | 10.05 | 0.217 | 0.65 | 0.054 | 0.115 |
| Heavy Duty Trucks | 2.68 | 0.095 | 7.95 | 0.171 | 1.20 | 0.100 | 0.113 |
| L-Category | 8.82 | 0.313 | 0.12 | 0.003 | 2.39 | 0.198 | 0.040 |
| Light Commercial Vehicles | 2.08 | 0.074 | 1.54 | 0.033 | 0.22 | 0.019 | 0.245 |
| Passenger Cars | 6.97 | 0.247 | 0.62 | 0.013 | 0.66 | 0.054 | 0.160 |

**Table S3.** Photochemical reactions and their reaction rate coefficients (J-values) at 293 K included in the Reduced Chemical Scheme (RCS).

| Order | Reactions | *J*-Values | Type |
|---|---|---|---|
| 1 | $O_3 \rightarrow OH + OH$ | $3.40 \times 10^{-6}$ | Inorganic |
| 2 | $H_2O_2 \rightarrow OH + OH$ | $7.11 \times 10^{-6}$ | Inorganic |
| 3 | $NO_2 \rightarrow NO + O_3$ | $9.20 \times 10^{-3}$ | Inorganic |
| 4 | $NO_3 \rightarrow NO$ | $2.34 \times 10^{-2}$ | Inorganic |
| 5 | $NO_3 \rightarrow NO_2 + O_3$ | $1.83 \times 10^{-1}$ | Inorganic |
| 6 | $HONO \rightarrow OH + NO$ | $2.02 \times 10^{-3}$ | Inorganic |
| 7 | $HNO_3 \rightarrow OH + NO_2$ | $6.30 \times 10^{-7}$ | Inorganic |
| 8 | $HCHO \rightarrow CO + HO_2 + HO_2$ | $3.05 \times 10^{-5}$ | Organic |
| 9 | $HCHO \rightarrow H_2 + CO$ | $4.61 \times 10^{-5}$ | Organic |
| 10 | $CH_3CHO \rightarrow CH_3O_2 + HO_2 + CO$ | $5.07 \times 10^{-6}$ | Organic |
| 11 | $CARB_7 = CH_3CO_3 + HCHO + HO_2$ | $3.36 \times 10^{-6}$ | Organic |
| 12 | $HOCH_2CHO = HCHO + CO + HO_2 + HO_2$ | $1.77 \times 10^{-5}$ | Organic |
| 13 | $UCARB10 = CH_3CO_3 + HCHO + HO_2$ | $1.62 \times 10^{-5}$ | Organic |
| 14 | $CARB6 = CH_3CO_3 + CO + HO_2$ | $1.26 \times 10^{-4}$ | Organic |
| 15 | $UCARB12 = CH_3CO_3 + HOCH_2CHO + CO + HO_2$ | $1.62 \times 10^{-5}$ | Organic |
| 16 | $CH_3NO_3 = HCHO + HO_2 + NO_2$ | $8.96 \times 10^{-7}$ | Organic |
| 17 | $CH_3OOH = HCHO + HO_2 + OH$ | $5.44 \times 10^{-6}$ | Organic |
| 18 | $CH_3CO_3H = CH_3O_2 + OH$ | $5.44 \times 10^{-6}$ | Organic |
| 19 | $HOCH_2CO_3H = HCHO + HO_2 + OH$ | $5.44 \times 10^{-6}$ | Organic |
| 20 | $RU14OOH = UCARB12 + HO_2 + OH$ | $1.37 \times 10^{-6}$ | Organic |
| 21 | $RU14OOH = UCARB10 + HCHO + HO_2 + OH$ | $4.07 \times 10^{-6}$ | Organic |
| 22 | $RU12OOH = CARB6 + HOCH_2CHO + OH$ | $5.44 \times 10^{-6}$ | Organic |
| 23 | $RU10OOH = CH_3CO_3 + HOCH_2CHO + OH$ | $5.44 \times 10^{-6}$ | Organic |
| 24 | $HOC2H4OOH = HCHO + HCHO + HO_2 + OH$ | $5.44 \times 10^{-6}$ | Organic |
| 25 | $RN9OOH = CH_3CHO + HCHO + HO_2 + OH$ | $5.44 \times 10^{-6}$ | Organic |

**Table S4.** Statistical evaluation of the MBM-FleX for $NO_2$, $NO_x$, and $O_3$ at different building heights within the deep street canyon (AR = 3.7).

| Case | Species | Location | n | FAC2 | r | RMSEs | RMSEu | RMSE | IOA |
|---|---|---|---|---|---|---|---|---|---|
| Case A1 | $NO_2$ | 3 m | 23 | 0.96 | 0.44 | 0.56 | 10.4 | 10.42 | −0.03 |
| | | 12 m | 25 | 0.88 | 0.74 | 2.55 | 6.24 | 6.74 | 0.28 |
| | $NO_x$ | 3 m | 23 | 0.52 | 0.5 | 26.72 | 13.6 | 29.98 | 0.04 |
| | | 12 m | 25 | 0.92 | 0.58 | 7.94 | 15.61 | 17.51 | 0.48 |
| | $O_3$ | 3 m | 23 | 0.01 | 0.61 | 81.32 | 35.03 | 88.54 | −0.98 |
| | | 12 m | 25 | 0.01 | 0.71 | 36.22 | 13.98 | 38.82 | −0.91 |
| Case A2 | $NO_2$ | 3 m | 23 | 0.48 | 0.47 | 12.48 | 4.01 | 13.1 | −0.27 |
| | | 12 m | 25 | 0.52 | 0.72 | 9.66 | 3.77 | 10.37 | −0.19 |
| | $NO_x$ | 3 m | 23 | 0.87 | 0.5 | 17.42 | 13.26 | 21.89 | 0.33 |
| | | 12 m | 25 | 0.96 | 0.59 | 7.74 | 13.86 | 15.88 | 0.57 |
| | $O_3$ | 3 m | 23 | 0.39 | 0.3 | 5.29 | 0.77 | 5.34 | −0.67 |
| | | 12 m | 25 | 0.44 | 0.57 | 5.69 | 0.8 | 5.74 | −0.44 |
| Case A3 | $NO_2$ | 3 m | 23 | 0.99 | 0.48 | 3.44 | 6.54 | 7.39 | 0.35 |
| | | 12 m | 25 | 0.99 | 0.71 | 1.24 | 5.16 | 5.3 | 0.4 |
| | $NO_x$ | 3 m | 23 | 0.87 | 0.44 | 17.55 | 14.95 | 23.06 | 0.29 |
| | | 12 m | 25 | 0.96 | 0.59 | 6.62 | 15.43 | 16.79 | 0.5 |
| | $O_3$ | 3 m | 23 | 0.65 | 0.76 | 1.73 | 2.33 | 2.91 | −0.2 |
| | | 12 m | 25 | 0.84 | 0.8 | 0.93 | 1.59 | 1.84 | 0.51 |
| Case A4 | $NO_2$ | 3 m | 23 | 0.99 | 0.48 | 3.99 | 4.23 | 5.81 | 0.43 |
| | | 12 m | 25 | 0.99 | 0.72 | 1.43 | 4.19 | 4.43 | 0.52 |
| | $NO_x$ | 3 m | 23 | 0.87 | 0.5 | 17.42 | 13.26 | 21.89 | 0.33 |
| | | 12 m | 25 | 0.96 | 0.59 | 7.74 | 13.86 | 15.88 | 0.57 |
| | $O_3$ | 3 m | 23 | 0.01 | 0.57 | 4.43 | 0.21 | 4.44 | −0.6 |
| | | 12 m | 25 | 0.04 | 0.68 | 4.28 | 0.67 | 4.33 | −0.25 |

**Table S5.** Statistical evaluation of the MBM-FleX_r for $NO_2$, $NO_x$, and $O_3$ within the deep street canyon (AR = 3.7).

| **Case** | Species | location | n | FAC2 | r | RMSEs | RMSEu | RMSE | IOA |
|---|---|---|---|---|---|---|---|---|---|
| Case C1 | $NO_2$ | total | 0.98 | 0.55 | 3.56 | 4.51 | 5.75 | 0.5 | 0.98 |
| | | 3 m | 0.96 | 0.43 | 5.03 | 4.61 | 6.82 | 0.37 | 0.96 |
| | | 12 m | 0.99 | 0.68 | 1.88 | 4.14 | 4.54 | 0.56 | 1 |
| | $NO_x$ | total | 0.79 | 0.49 | 16.88 | 13.64 | 21.7 | 0.54 | 0.79 |
| | | 3 m | 0.7 | 0.62 | 22.16 | 12.97 | 25.68 | 0.19 | 0.7 |
| | | 12 m | 0.88 | 0.46 | 11.31 | 13.04 | 17.26 | 0.57 | 0.88 |
| | $O_3$ | total | 0.04 | 0.22 | 3.96 | 1.9 | 4.4 | −0.4 | 0.04 |
| | | 3 m | 0.04 | 0.74 | 3.6 | 0.58 | 3.65 | −0.51 | 0.04 |
| | | 12 m | 0.04 | 0.08 | 4.3 | 2.52 | 4.99 | −0.35 | 0.04 |
| Case C2 | $NO_2$ | total | 0.98 | 0.55 | 3.56 | 4.51 | 5.75 | 0.5 | 0.98 |
| | | 3 m | 0.96 | 0.43 | 5.03 | 4.61 | 6.82 | 0.37 | 0.96 |
| | | 12 m | 0.99 | 0.68 | 1.88 | 4.14 | 4.54 | 0.56 | 0.99 |
| | $NO_x$ | total | 0.79 | 0.49 | 16.88 | 13.64 | 21.7 | 0.54 | 0.79 |
| | | 3 m | 0.7 | 0.62 | 22.16 | 12.97 | 25.68 | 0.19 | 0.7 |
| | | 12 m | 0.88 | 0.46 | 11.31 | 13.04 | 17.26 | 0.57 | 0.88 |
| | $O_3$ | total | 0.04 | 0.22 | 3.96 | 1.9 | 4.4 | −0.4 | 0.04 |
| | | 3 m | 0.04 | 0.74 | 3.6 | 0.58 | 3.65 | −0.51 | 0.04 |
| | | 12 m | 0.04 | 0.08 | 4.3 | 2.52 | 4.99 | −0.35 | 0.04 |
| Case C3 | $NO_2$ | total | 0.98 | 0.59 | 3.14 | 4.75 | 5.7 | 0.48 | 0.98 |
| | | 3 m | 0.96 | 0.44 | 4.11 | 4.86 | 6.36 | 0.4 | 0.96 |
| | | 12 m | 0.99 | 0.66 | 2.11 | 4.53 | 5 | 0.49 | 0.99 |
| | $NO_x$ | total | 0.85 | 0.58 | 16.11 | 12.95 | 20.67 | 0.57 | 0.85 |
| | | 3 m | 0.78 | 0.58 | 20.59 | 12.89 | 24.29 | 0.26 | 0.78 |
| | | 12 m | 0.92 | 0.53 | 10.72 | 12.74 | 16.65 | 0.59 | 0.92 |

| **Case** | Species | location | n | FAC2 | r | RMSEs | RMSEu | RMSE | IOA |
|---|---|---|---|---|---|---|---|---|---|
| | | total | 0.77 | 0.86 | 1.04 | 1.31 | 1.67 | 0.45 | 0.77 |
| | $O_3$ | 3 m | 0.7 | 0.79 | 1.16 | 1.41 | 1.83 | 0.08 | 0.7 |
| | | 12 m | 0.84 | 0.9 | 1.01 | 1.14 | 1.52 | 0.61 | 0.84 |
| | | total | 0.98 | 0.55 | 3.56 | 4.51 | 5.75 | 0.5 | 0.98 |
| | $NO_2$ | 3 m | 0.96 | 0.43 | 5.03 | 4.61 | 6.82 | 0.37 | 0.96 |
| | | 12 m | 0.99 | 0.68 | 1.88 | 4.14 | 4.54 | 0.56 | 0.99 |
| | | total | 0.79 | 0.49 | 16.88 | 13.64 | 21.7 | 0.54 | 0.79 |
| Case C4 | $NO_x$ | 3 m | 0.7 | 0.62 | 22.16 | 12.97 | 25.68 | 0.19 | 0.7 |
| | | 12 m | 0.88 | 0.46 | 11.31 | 13.04 | 17.26 | 0.57 | 0.88 |
| | | total | 0.04 | 0.22 | 3.96 | 1.9 | 4.4 | −0.4 | 0.04 |
| | $O_3$ | 3 m | 0.04 | 0.74 | 3.6 | 0.58 | 3.65 | −0.51 | 0.04 |
| | | 12 m | 0.04 | 0.08 | 4.3 | 2.52 | 4.99 | −0.35 | 0.04 |

## References


1. Bright, V.B.; Bloss, W.J.; Cai, X. Urban street canyons: Coupling dynamics, chemistry and within-canyon chemical processing of emissions. *Atmos. Environ.* **2013**, *68*, 127–142.
2. Zhong, J.; Cai, X.-M.; Bloss, W.J. Modelling the dispersion and transport of reactive pollutants in a deep urban street canyon: Using large-eddy simulation. *Environ. Pollut.* **2015**, *200*, 42–52.
3. Dai, Y.; Cai, X.; Zhong, J.; MacKenzie, A.R. Modelling chemistry and transport in urban street canyons: Comparing offline multi-box models with large-eddy simulation. *Atmos. Environ.* **2021**, *264*, 118709.
4. Zhong, J.; Cai, X.-M.; Bloss, W.J. Modelling segregation effects of heterogeneous emissions on ozone levels in idealised urban street canyons: Using photochemical box models. *Environ. Pollut.* **2014**, *188*, 132–143.
5. Li, C.W.; Brasseur, G.P.; Schmidt, H.; Mellado, J.P. Error induced by neglecting subgrid chemical segregation due to inefficient turbulent mixing in regional chemical-transport models in urban environments. *Atmos. Chem. Phys.* **2021**, *21*, 483–503.